Carbon adsorbents for CO_2 capture from bio-hydrogen and biogas streams: Breakthrough adsorption study

M.V. Gil[a,b], N. Álvarez-Gutiérrez[a], M. Martínez[a], F. Rubiera[a], C. Pevida[a,*], A. Morán[b]

[a] *Instituto Nacional del Carbón, INCAR-CSIC, Apartado 73, 33080 Oviedo, Spain*

[b] *Chemical Engineering Department, IRENA, University of León, Avda. de Portugal 41, 24071 León, Spain*

Abstract

The biological production of H_2 by dark fermentation is being extensively investigated due to the great potential of the two-phase hydrogen/methane fermentation process for recovering energy from carbohydrate-rich wastes. However, the purification of the bio-hydrogen and biogas obtained is needed to produce high-purity H_2 and CH_4 streams appropriate for industrial application. In this study, the performance of three activated carbons (No1KCla-600, No1KClb-1000 and No2OS-1000), synthesized from phenol-formaldehyde resins, as potential adsorbents for CO_2 capture from bio-hydrogen and biogas streams has been evaluated under dynamic conditions. Adsorption-desorption cycles by means of temperature swings were conducted at ambient temperature and atmospheric pressure with CO_2/H_2 (40/60 and 70/30 vol.% at normal conditions) and CO_2/CH_4 (50/50 vol.% at normal conditions) binary gas mixtures in a purpose-built fixed-bed set-up. The performance of the resin-derived carbons to separate CO_2 was superior to that of reference commercial carbons in terms of CO_2 uptake, breakthrough time and column efficiency. These adsorbents presented high

*Corresponding author. Tel.: +34 985 119 090; Fax: +34 985 297 662

E-mail address: cpevida@incar.csic.es (C. Pevida)

CO_2/H_2 and CO_2/CH_4 selectivity values, were easily completely regenerated and did not show capacity decay after multiple cycling. Breakthrough capacities reached 2.11 and 2.03 mmol g^{-1} at 25 ºC for 70/30 CO_2/H_2 and 50/50 CO_2/CH_4, respectively. The No2OS-1000 adsorbent, produced from phenol-formaldehyde resin and olive stones (20:80 wt.), gave the greatest values of CO_2 capture capacity on a volumetric basis and CO_2/CH_4 selectivity, which may be advantageous to biogas purification applications because it reduces the size of the necessary equipment.

Keywords: Bio-hydrogen; Biogas; Dark fermentation; Activated carbon; CO_2 capture; Breakthrough test

1. Introduction

Hydrogen is currently recognised as a clean energy carrier for the future energy economy. Amongst the variety of alternatives available for its generation, the hydrogen production by biological means, although still far from being a commercially viable technology, shows great promise for the future [1]. Biological approaches could contribute to large-scale hydrogen production as various microorganisms can produce H_2 under moderate conditions from readily available, renewable substrates, making biological strategies potentially competitive with chemical processes such as reforming and gasification. Bio-hydrogen processes are 'CO_2-neutral', being fuelled by carbohydrates originated from photosynthetic fixation of CO_2 [2]. Within the different microbial processes which use microorganisms capable of forming H_2, the dark fermentation is one of the technologies that has been investigated with a focus on bio-hydrogen production due to its ability to produce hydrogen continuously from a number

of renewable feedstocks, such as biomass-derived sugars, organic wastes, and carbohydrate-rich wastewater, without an input of external energy [3, 4]. Thus, the dark fermentation technology has successfully been used to treat residual biomass sources [1, 5-8] in order to recover hydrogen gas. These works indicated that two-phase hydrogen/methane fermentation process may have a great potential for recovering energy from carbohydrate-rich wastes. Gómez et al. [4] pointed out that the dark fermentation process is the only biological method of hydrogen production with a prospect of being rapidly scaled-up owing to its similarities to the well-known and in use at full-scale anaerobic digestion process.

Anaerobic fermentation is mediated by two major types of bacteria: acidogenic bacteria that break down substrates into primarily H_2, acetic acid, and CO_2; and methanogenic bacteria that convert them to methane gas. Such two-phase fermentation method has been proposed to optimize the growth of each type of bacteria in separate reactors. Then, the hydrogen produced in the acidogenic fermentation and the methane obtained during the methanogenic fermentation may be recovered [9]. In the last years, several authors have investigated the two-phase fermentation process to produce H_2 and methane simultaneously from food wastes [9-14]. The concentration of H_2 in the gas generated in the hydrogen fermentation reactor can reach values of up to 30-70 vol.% on average. Likewise, the produced biogas from the methane fermentation reactor can reach values of up to 45-80 vol.% of CH_4 on average. The presence of CO_2 on both streams (20-70 vol.%) is undesirable for further utilization of H_2 and CH_4. Thus, CO_2 needs to be separated and concentrated to allow the efficient exploitation of the bio-hydrogen and biogas produced.

Different technologies have been proposed to separate CO_2 from biogas streams [15]. These techniques include chemical absorption by water washing or amine scrubbing [16, 17], membrane separation [18-20] and physical adsorption by temperature swing adsorption (TSA) or pressure swing adsorption (PSA) [21-24]. Amine scrubbing is the most economical upgrading process, but only for high flow rates. For smaller size plants, pressure swing adsorption (PSA) technologies using solid adsorbents are proposed [25]. Vacuum pressure-swing adsorption (VPSA) also seems to be a suitable process for locations with small to medium flow rates under mild temperatures [26].

On the other hand, separation of CO_2 from biological hydrogen obtained by dark fermentation has been hardly explored, and the published works are based on membrane systems, in which the gas mixture must be previously compressed [27-29]. However, PSA units are commonly used in the purification of hydrogen produced from natural gas steam reforming [30] and they are able to produce very pure H_2 by removing relatively high concentrations of CO_2. Adsorption by biomass-derived activated carbons was proposed for the purification of hydrogen from a gas stream generated from the dark fermentation process in a previous work carried out in collaboration with the University of León [1] and the results demonstrated a successful separation of CO_2. However, the authors highlighted that the success of this approach is dependent on the development of low-cost adsorbents with a high CO_2 selectivity and adsorption capacity and with a good performance in multiple adsorption/desorption cycles.

A wide variety of solid sorbents has been and is currently being investigated to separate CO_2 from gas streams, such as zeolites, activated carbons, calcium oxides, hydrotalcites, supported amines and metal-organic framework (MOF) materials.

Zeolites are the most extensively studied and commercially used CO_2 adsorbents, due to their stability at high temperatures and pressures and high selectivity to CO_2. Many of the published works on the separation of CO_2 from biogas streams are based on adsorption on zeolites [21, 23, 31-33]. However, activated carbons show a high adsorption capacity at atmospheric pressure and present important advantages over zeolites, such as their hydrophobicity, their significant lower cost and the lower amount of energy required to regenerate them. Phenol-formaldehyde resin-derived microporous activated carbons have been previously prepared in our laboratory and they have been successfully applied as CO_2 adsorbents under high pressure CO_2/H_2 gas streams [34, 35]. Therefore, adsorption with phenolic resin-derived activated carbons could also be a promising technology to separate and concentrate CO_2 from CO_2/H_2 and CO_2/CH_4 gas streams at atmospheric pressure and to obtain high purity hydrogen and methane, respectively. Phenolic resins constitute a family of low-cost polymers, one of the most common being those produced from phenol and formaldehyde [36]. Phenolic resin-derived activated carbons offer further advantages in that they can be produced in a wide variety of physical forms (e.g., granular or extruded, as fibres or as monolithic structures), they allow a close control of porosity and present a very low level of impurities and good physical strength [37, 38]. On the other hand, biomass residues, such as olive stones, are also a low-cost and relatively abundant by-product that can be used as a feedstock for the successful production of microporous activated carbons [39-41]. Previous research conducted in our laboratory has successfully proved the potential of olive stones based carbons for post-combustion CO_2 capture [42, 43].

A high CO_2 adsorption capacity coupled with a high CO_2/H_2 or CO_2/CH_4 selectivity will be key properties of an adsorbent material for the separation of CO_2

from bio-hydrogen or biogas streams. Most of the literature on CO_2 capture with solid sorbents is based on equilibrium CO_2 adsorption capacities, determined from CO_2 adsorption isotherms at the desired temperature [44-46]. However, the suitability of an adsorbent for CO_2 capture relies on efficient regeneration and cycling, since solid adsorbents are typically used in cyclic, multi-module processes of adsorption and desorption, with desorption being induced by a swing in pressure and/or temperature [47].

Thus, in the present work three microporous activated carbons have been synthesized using phenol-formaldehyde resins and olive stones as precursor materials. The performance of the adsorbents to separate CO_2 from CO_2/H_2 and CO_2/CH_4 binary mixtures in a temperature swing adsorption (TSA) process at atmospheric pressure has been evaluated by means of breakthrough adsorption tests conducted in a purpose-built lab-scale fixed-bed unit. Additionally, two commercial activated carbons (Calgon BPL and Norit C) were evaluated under the same operating conditions to be used as reference carbon adsorbents.

2. Materials and methods

2.1. Materials

Three activated carbons (No1KCla-600, No1KClb-1000 and No2OS-1000) prepared in our laboratory from *Novolac* phenol-formaldehyde resins and olive stones (OS), a low-cost biomass residue from the Spanish food industry, have been evaluated as adsorbent materials. Moreover, two commercial activated carbons, Calgon BPL and Norit C, were also tested for comparison purposes.

Calgon BPL is a bituminous coal-based carbon activated at a high temperature with steam. It shows an apparent BET surface area of 1129 m^2 g^{-1} and a total pore volume of 0.50 cm^3 g^{-1}. Norit C is a wood-based granular carbon manufactured by phosphoric acid activation. It shows an apparent BET surface area of 1361 m^2 g^{-1} and a total pore volume of 0.97 cm^3 g^{-1}.

No1KCla-600, No1KClb-1000 and No2OS-1000 were prepared by a first step of carbonization under inert atmosphere, followed by activation in CO_2 atmosphere. Details on the synthesis of these materials have been reported elsewhere [48]. Accordingly, the temperature and burn-off degree values used in the activation step were as follows: 810º C and 22% burn-off degree for No1KCla-600; 800º C and 20% burn-off degree for No1KClb-1000; and 940º C and 38% burn-off degree for No2OS-1000.

2.2. Characterization of materials

The carbons were characterized by physical adsorption of N_2 at -196 ºC and CO_2 at 0 ºC using a Micromeritics TriStar 3000 volumetric apparatus. The samples were outgassed overnight at 100ºC under vacuum prior to adsorption measurements. The total pore volume was estimated from the amount of nitrogen adsorbed at a relative pressure of 0.99. The micropore volume was determined by the Dubinin-Radushkevich (DR) equation [49]. The average micropore width was calculated by means of the Stoeckli-Ballerini relation [50]. The apparent surface area was estimated from the N_2 adsorption isotherms at -196 ºC by means of the Brunauer–Emmett–Teller (BET) equation [51]. The apparent density was determined at 0.1 MPa in a Micromeritics Autopore IV 9500

mercury porosimeter. The helium density was measured in an Accupyc 1330 apparatus at 35 ºC.

Table 1 summarizes the main characteristics of the evaluated adsorbents. No1KCla-600, No1KClb-1000 and No2OS-1000 present apparent BET surface areas (1091, 804 and 1233 m^2 g^{-1}, respectively) close to that of Calgon BPL, high carbon contents (99, 99 and 98 wt.%, respectively) and well-developed microporosity (N_2-micropore volume of 0.43, 0.32 and 0.50 cm^3 g^{-1}, respectively, assessed from the DR equation applied to the N_2 adsorption isotherms at -196 ºC). Narrow micropore volumes (determined from the DR relation applied to the CO_2 adsorption isotherms at 0 ºC) account for the majority of the microporosity (70-85%) in the produced carbons. This parameter has been pointed out as critical to the CO_2 adsorption capacity of solid sorbents at atmospheric pressure [52].

2.3. Breakthrough adsorption experiments with CO_2/H_2 and CO_2/CH_4 binary mixtures in a fixed-bed reactor

In order to evaluate the performance of the studied adsorbents to separate CO_2 from CO_2/H_2 and CO_2/CH_4 gas streams, breakthrough experiments with binary gas mixtures were conducted in a purpose-built fixed-bed adsorption unit (Fig. 1). The detailed description of the adsorption unit has been reported previously [53]. The column was packed with the activated carbons in order to measure the dynamics of adsorption of CO_2, H_2 and CH_4 during the experiments. The composition of the outlet gas stream was analysed by a dual channel micro-chromatograph, Varian CP-4900, equipped with a thermal conductivity detector (TCD) in which He and Ar were used as the carrier gases. The main characteristics of the adsorbent beds are summarized in

Table 1. Breakthrough tests consisted in consecutive adsorption-desorption cycles: the adsorbent reached saturation (maximum adsorption capacity of the adsorbed components) during the adsorption step and it was completely regenerated during the desorption step.

In a representative cyclic adsorption-desorption experiment (Fig. 2), the adsorbent was dried (i.e., cleaned) by flowing inert gas (50 mL min^{-1} STP) for 50 min at 100 ºC and 120 kPa. N_2 was used as inert gas in the experiments with CO_2/H_2 mixtures, whereas He was selected for the experiments with CO_2/CH_4 mixtures. After the drying step, the bed was cooled down to the adsorption temperature (25 ºC) under inert gas atmosphere. Then, the adsorption step was launched feeding the selected CO_2/H_2 (40%CO_2-60%H_2 or 70%CO_2-30%H_2) or CO_2/CH_4 (50%CO_2-50%CH_4) gas stream -representative to the concentrations attained in a dark fermentation process- to the pre-conditioned column, filled with inert gas at the adsorption temperature and pressure, for 60 min. A total feed gas flow rate of 30 mL min^{-1} STP was kept constant during the adsorption step. The CO_2 and H_2, or CH_4, concentrations in the gas stream exiting the adsorption column were continuously monitored as a function of time (breakthrough curve) until the composition approached the inlet gas composition set point, i.e., until saturation was reached. The adsorbed CO_2 was completely desorbed by raising the temperature of the bed to 80 ºC –similarly to a temperature swing adsorption operation– under inert gas atmosphere for 60 min. The adsorbent bed was subjected to six consecutive adsorption-desorption cycles and the maximum adsorption capacity of the adsorbent for each component in the feed stream and the breakthrough time under the tested conditions were assessed.

Examples of a complete breakthrough adsorption experiment for 40/60 vol.% CO_2/H_2 and 50/50 vol.% CO_2/CH_4 binary feed gas mixtures are shown in Figs. 3 and 4, respectively. The outlet gas concentrations and the bed temperature profiles for the six consecutive adsorption-desorption cycles are shown. The first step (1) corresponds to the initial drying at 100 ºC under inert gas flow and the second step (2) to the pre-conditioning of the adsorbent bed with a decrease in temperature under inert gas flow. The third step (3) corresponds to the adsorption stage, in which the CO_2/H_2 or CO_2/CH_4 gas mixtures are fed into the adsorbent bed at 25 ºC and 120 kPa. The last step (4) corresponds to the desorption stage, where the bed is heated up to 80 ºC under inert gas flow to achieve complete regeneration of the adsorbent bed. The adsorption step (3) is characterized by zero CO_2 (and CH_4) outlet gas concentrations at the beginning while these components are being adsorbed. When the breakthrough time is reached, an increase in CO_2 (or CH_4) concentration is observed. Once the bed is fully saturated, the outlet gas concentrations return to the inlet conditions. H_2 adsorption on the carbons is negligible and its concentration profile remains unchanged throughout the adsorption stage. During the desorption step (4), the previously adsorbed CO_2 or CH_4 starts to desorb. The raise in temperature results in a sharp increase in the outlet CO_2 concentration at the beginning of the regeneration step of the CO_2/H_2 runs, which progressively decreases to nearly zero at the end (Fig. 3). This is due to the strength of the CO_2 adsorption when compared to H_2. In the case of the CO_2/CH_4 runs (Fig. 4), both CO_2 and CH_4 show a gradual decrease in the outlet concentration.

The capture capacity was evaluated as an average of the adsorption performance of the adsorbents after six consecutive adsorption-desorption cycles. A mass balance was applied to the bed in each adsorption-desorption cycle to calculate the specific

amount of the component *i* (CO_2, H_2 or CH_4) adsorbed at equilibrium (q_i), as illustrated in Equation (1):

(A) (B) (C)

$$q_i = \frac{1}{m_{\text{adsorbent}}}\left[\int_0^{t_s}\left(F_{i,\text{feed}} - F_{i,\text{out}}\right)\mathrm{d}t - \frac{y_{i,\text{feed}}P_\text{b}\varepsilon_\text{T}V_\text{b}}{ZRT_\text{b}} - \frac{y_{i,\text{feed}}P_\text{b}V_\text{d}}{ZRT_\text{b}}\right] \quad (1)$$

where q_i is the specific adsorption capacity of the adsorbent for the component *i*; $m_{\text{adsorbent}}$ is the mass of adsorbent in the bed; $F_{i,\text{feed}}$ and $F_{i,\text{out}}$ are the molar flow rates of the component *i* at the inlet and outlet of the bed, respectively; t_s is the time required to reach saturation; $y_{i,\text{feed}}$ is the molar fraction of the component *i* in the feed stream; P_b and T_b are the pressure and temperature of the bed at equilibrium; ε_T is the total porosity of the bed; V_b is the bed volume; V_d is the dead volume in the system (tubing + column); *Z* is the compressibility factor of the component *i* at P_b and T_b; and *R* is the universal gas constant. In the present work, t_s is the time at which the bed is completely saturated, which means that the concentration of the component *i* at the bed outlet equals the feed concentration ($y_{i,\text{out}} = y_{i,\text{feed}}$).

The total porosity of the bed, ε_T, is calculated by means of the following equation:

$$\varepsilon_\text{T} = \varepsilon_\text{b} + (1 - \varepsilon_\text{b})\,\varepsilon_\text{p} \quad (2)$$

where ε_b is the packed bed porosity and ε_p is the particle porosity.

In Equation (1), the term (A) is the total number of moles of the component *i* retained in the system over the cycle time and it can be calculated by a graphical method that makes use of the outlet concentration of the component *i* and the total molar flow rate at each time *t* between 0 and t_s. Terms (B) and (C) are correction factors to account

for the gas component *i* which has accumulated in the interstitial voids and dead space of the system, respectively.

3. Results and discussion

Breakthrough adsorption experiments for the activated carbons Calgon BPL, Norit C, No1KCla-600, No1KClb-1000 and No2OS-1000 were carried out at 25 ºC and 120 kPa, where the feed gas containing a constant CO_2 concentration was passed through the adsorption column. The progress of the effluent gas concentration exiting the bed, i.e., its breakthrough curve, was recorded. The equilibrium CO_2 adsorption capacity and the breakthrough time (t_b), i.e., the time it takes for CO_2 to be detected at the adsorption column outlet, were calculated to estimate the CO_2 column dynamics. The breakthrough experiments were conducted until saturation was reached, i.e., until the outlet CO_2 concentration equals that of the inlet stream, in order to assess the maximum dynamic adsorption capacity of the adsorbent [53]. During the desorption step the adsorbent was fully regenerated with hot inert gas so that the repeatability of the breakthrough curves could be assessed.

The concentration profiles of H_2 in Fig. 3 show that this component is detected from the beginning of the adsorption step since it is not adsorbed on the solids bed, while CO_2 is not detected over a period of time and thus adsorbed. This behaviour points out the selectivity of the studied carbons to separate CO_2 from CO_2/H_2 mixtures. However, Fig. 4 shows that neither CO_2 nor CH_4 are detected at the beginning of the adsorption step, which indicates adsorption of both gases. After a short time, the outlet CH_4 concentration increases, indicating that desorption of this gas starts while CO_2 is still being adsorbed on the adsorbent bed. In addition, the outlet CH_4 concentration goes

beyond the CH_4 feed gas concentration. This is due to the ability of CO_2 to replace the CH_4 adsorbed in the bed. This phenomenon is called *roll-up* or *roll-over*, i.e., the molar flow rate of CH_4 in the effluent is temporally higher than that fed to the adsorption bed. It will be further analysed in section 3.2.

These concentration profiles clearly indicate that CO_2 is much more adsorbed than CH_4 and more significantly than H_2 on the tested carbons. In terms of equilibrium of adsorption, CO_2 holds a larger quadropole moment that produces a strong attraction to the adsorbent surface resulting in a greater adsorbed amount. The high level of polarizability of CO_2 and CH_4 can create a momentary shift in its neutral electrostatic field but this attraction force is much weaker than the quadrupole moment.

The CO_2 and CH_4 breakthrough curves were measured for the activated carbons under study and C/C_0 (ratio between the outlet CO_2 or CH_4 concentration at a given time and that in the feed) was plotted versus time for the CO_2/H_2 (Fig. 5) and CO_2/CH_4 (Figs. 6 and 7) experiments. The breakthrough times were taken at a relative concentration ($C_{i,outlet}/C_{i,feed}$) of 0.05. As shown in Figs. 5-7, consecutive CO_2 breakthrough curves practically overlap showing that regeneration was homogeneous over the cycles and the performance of the adsorbent was not altered. Therefore, CO_2 capture over the six consecutive temperature swing adsorption-desorption cycles can be considered stable. Table 2 shows the CO_2 and CH_4 adsorption capacities and the breakthrough times from the breakthrough experiments at 25 ºC and 120 kPa for the studied activated carbons.

3.1. Breakthrough curves from adsorption experiments with CO_2/H_2

The performance of the adsorbents for separating CO_2 from the CO_2/H_2 gas stream was conducted under two CO_2 partial pressures (40%CO_2-60%H_2 and 70%CO_2-30%H_2 gas mixtures). In these experiments (Fig. 5), the commercial activated carbons showed shorter breakthrough at both CO_2 partial pressures studied. The breakthrough times followed the order: Norit C << Calgon BPL < No2OS-1000 < No1KClb-1000 < No1KCla-600 (Table 2). Thus, under the same experimental conditions, Norit C and Calgon BPL beds became saturated earlier. It should be pointed out that Norit C showed very low breakthrough times (2.3 and 1.6 min for 40%CO_2-60%H_2 and 70%CO_2-30%H_2 gas mixtures, respectively) compared to the other adsorbents, whose breakthrough times were above 5 min for the 40%CO_2-60%H_2 mixture and above 4 min for the 70%CO_2-30%H_2 mixture. Moreover, at a given adsorption temperature, a higher CO_2 concentration in the feed (i.e., a higher CO_2 partial pressure) resulted in a shorter breakthrough time (Table 2) for all the carbon adsorbents, indicating that the CO_2 concentration front took less time to reach the outlet of the bed.

The efficiency of the adsorbent bed, due to mass transfer resistance during adsorption, can be estimated from the percentage of unused bed. It can be calculated by Equation (3) as follows:

$$\%\ \text{unused bed} = 1 - \frac{q_{CO_2,b}}{q_{CO_2}} \tag{3}$$

where $q_{CO_2,b}$ and q_{CO_2} stand for the mol of CO_2 adsorbed up to the break point and up to saturation of the bed, respectively. For the experiments with CO_2/H_2 binary mixtures, the highest percentages of unused bed were observed with the commercial activated carbons. The percentage of unused bed followed the order: Norit C >> Calgon BPL > No2OS-1000 > No1KClb-1000 > No1KCla-600 (Table 2). According to Equation (3),

the percentage of unused bed may evaluate the efficiency of the adsorbent bed, because the closer the values of $q_{CO_2,b}$ and q_{CO_2} the narrower the mass transfer zone is. The results therefore indicate that the column was more inefficient using the commercial activated carbons, particularly Norit C. A better efficiency of utilization due to a higher mass transfer along the adsorbent bed was observed for the synthesized phenol-formaldehyde resin-derived activated carbons, particularly in the case of No1KCla-600 and No1KClb-1000.

3.2. Breakthrough curves from adsorption experiments with CO_2/CH_4

The breakthrough curves obtained for CO_2/CH_4 binary feed gas mixtures are shown in Fig. 6, for the tested activated carbons. A roll-up can be observed in the CH_4 breakthrough curve due to the preferential adsorption of CO_2 over CH_4. At this point, the outlet CH_4 concentration reaches a value twice that of the inlet CH_4 concentration in the feed to the column. This effect is explained by the molecules of CO_2 (strong adsorbate) being able to replace the molecules of CH_4 (weaker adsorbate). In addition, the diffusivity of CH_4 is higher than that of CO_2, which could also contribute to the roll-up phenomenon. The slopes of the CH_4 and CO_2 breakthrough curves are rather steep which may indicate that the substitution of CH_4 by CO_2 in the adsorbed phase is quite fast.

In Fig. 7 the breakthrough curves of the experiments with 50/50 vol.% CO_2/CH_4 in the feed gas for all the activated carbons studied have been overlapped for comparison purposes. Fig. 7a shows the CO_2 breakthrough curves, while Fig. 7b presents the CH_4 breakthrough curves. Following the same pattern of the CO_2/H_2 breakthrough experiments, the commercial activated carbons presented much shorter

CO_2 breakthrough times (2.1-3.4 min, in Table 2) than those of the synthesized adsorbents (5.5-6.7 min, in Table 2). The breakthrough times followed the order: Norit C < Calgon BPL << No2OS-1000 < No1KClb-1000 < No1KCla-600 (Table 2). This means that, under the same experimental conditions, phenol-formaldehyde resin-derived activated carbons beds take longer times to become saturated than the commercial activated carbons.

Moreover, analysing the shape of the CO_2 breakthrough curves (Fig. 7a) in more detail, it is observed that Calgon BPL and No2OS-1000 display more distended mass transfer zones (between the break point and saturation) than Norit C, No1KCla-600 and No1KClb-1000 activated carbons. This indicates that mass-transfer for the latter three carbons may be faster. A narrow mass-transfer zone is suitable to make efficient use of the adsorbent bed and to reduce the energy costs associated to the subsequent regeneration.

On the other hand, the difference between the CO_2 and CH_4 breakthrough times was much lower for the commercial activated carbons (around 1.1-1.2) compared to the synthesized adsorbents (2.6-2.8). The higher the difference between the CO_2 and CH_4 breakthrough times, the higher the separation effectiveness. This parameter may supply significant information, since its value could condition a possible kinetics-based separation using the prepared activated carbons.

3.3. Equilibrium adsorption capacity from dynamic experiments

The equilibrium dynamic capacity was determined from the breakthrough curves and the CO_2 and CH_4 capture capacities of the studied adsorbents are shown in Table 2. These values stand for the average CO_2 capture capacity over the six consecutive cycles

conducted in each experiment. While gravimetric capacities (mmol of CO_2 adsorbed per g of adsorbent) are usually reported in the literature when evaluating materials for CO_2 capture, the volumetric capacities (kg of CO_2 adsorbed per m^3 of adsorbent) were also calculated, since both parameters are critical in designing adsorption separation processes [35].

In the case of the CO_2/H_2 experiments for feed gas streams containing 40 and 70 vol.% of CO_2, respectively, the CO_2 adsorption capacity on a mass basis followed the order: Norit C < Calgon BPL < No2OS-1000 < No1KClb-1000 < No1KCla-600. This uptake is proportional to the breakthrough time, so the highest adsorption capacity corresponds to the longest breakthrough time, as it was also observed by García et al. [53] in their experiments of CO_2 separation from shifted-syngas streams. The performance of the synthesized adsorbents was superior to that of the commercial activated carbons: the average CO_2 capture capacities evaluated from these breakthrough tests were 1.0-1.1 mmol CO_2 g^{-1} for feed gas streams containing 40%CO_2-60%H_2, compared to 1.2, 1.5 and 1.6 mmol CO_2 g^{-1} for No2OS-1000, No1KClb-1000 and No1KCla-600, respectively, under the same conditions. For feed gas streams containing 70%CO_2-30%H_2, the average CO_2 capture capacities of the commercial activated carbons were 1.0-1.5 mmol CO_2 g^{-1}, whereas those of the synthesized adsorbents were 1.7, 2.0 and 2.1 mmol CO_2 g^{-1} for No2OS-1000, No1KClb-1000 and No1KCla-600, respectively. As expected, the CO_2 adsorption capacity of the activated carbons increased with the CO_2 partial pressure in the feed gas stream. Redondas et al. [1] carried out breakthrough tests with a biomass-derived activated carbon to separate CO_2 at atmospheric pressure from a CO_2/H_2 gas stream generated from the dark fermentation process of food wastes. Values of CO_2 capture capacities in the same

order, although slightly higher, than in the present work were reported (2.5 and 3.2 mmol CO_2 g^{-1} for feed gas streams containing 70 and 80% of CO_2, respectively). However, those tests were not performed under cyclic operation. In the present work, the greatest CO_2 adsorption capacity assessed from the adsorption-desorption cycles corresponded to the phenol-formaldehyde resin-derived adsorbent activated at 600 ºC, i.e., No1KCla-600.

On the other hand, on a volumetric basis the CO_2 adsorption capacity for feed gas stream containing both 40%CO_2-60%H_2 and 70%CO_2-30%H_2 followed the order: Norit C << No1KClb-1000 < Calgon BPL < No1KCla-600 < No2OS-1000. In this case, the CO_2 capture capacity of Norit C was also very low compared to that of the other adsorbents, whereas the adsorption capacity of Calgon BPL was similar to that of the phenol-formaldehyde resin-derived synthesized carbons. It should also be highlighted that the highest values of CO_2 adsorption capacity on a volumetric basis were obtained for No2OS-1000. The change in the trend observed when a volumetric basis is considered is due to the greater bed density of Calgon BPL and No2OS-1000 activated carbons.

In the case of the CO_2/CH_4 experiments, the CO_2 adsorption capacity on a mass basis followed the order: Calgon BPL ~ Norit C < No2OS-1000 < No1KClb-1000 < No1KCla-600 (Table 2). For both commercial activated carbons the average CO_2 capture capacities were around 1.5 mmol CO_2 g^{-1}, whereas for the synthesized adsorbents the average CO_2 adsorption capacities were 1.8, 1.9 and 2.0 mmol CO_2 g^{-1} for No2OS-1000, No1KClb-1000 and No1KCla-600, respectively. The highest CO_2 adsorption capacity was also obtained with the carbon activated at 600 ºC. On the other hand, the CH_4 adsorption capacity on a mass basis showed the following order: No2OS-

1000 ~ Norit C ~ Calgon BPL < No1KClb-1000 < No1KCla-600 (Table 2). It is worth to point out the lower CH_4 capture capacity of the biomass-derived adsorbent, No2OS-1000.

Comparing the CO_2/CH_4 results on a volumetric basis results in the following trend regarding the CO_2 adsorption capacity: Norit C << No1KClb-1000 < No1KCla-600 ~ Calgon BPL < No2OS-1000, which is also attributed to the greater bed density in the case of the No2OS-1000 and Calgon BPL activated carbons. Similarly to previously observed in the CO_2/H_2 experiments, the highest value of CO_2 adsorption capacity on a volumetric basis belongs to No2OS-1000. The CH_4 adsorption capacity follows similar trends on both volumetric and mass bases.

Most of the literature on CO_2/H_2 and CO_2/CH_4 separation by means of adsorption with solids sorbents is based on equilibrium CO_2 adsorption capacities determined from CO_2 adsorption isotherms or on molecular simulations to predict the adsorption capacity, where the activated carbons are not validated under cyclic operation. Adsorption isotherms do not consider any dispersive effect due to the packing of the adsorbent in the fixed-bed. Literature on the dynamic performance of adsorbent beds is scarce and, to the best of our knowledge, there are no references in the literature to activated carbons being tested under similar operational conditions to those presented herein. In the case of a CO_2/H_2 mixture, capture capacities of 1-2 mmol CO_2 g^{-1} have been reported [54, 55] at lower CO_2 partial pressures than those of the present work. Higher CO_2 partial pressures are encountered in the available literature for CO_2/H_2 and CO_2/CH_4 mixtures when high pressure systems are to be evaluated and the results cannot therefore be compared straightforward. However, the results of the present study indicate that the synthesized phenol-formaldehyde resin-derived

adsorbents show significant potential to capture CO_2 from bio-hydrogen and biogas streams generated by dark fermentation.

3.4. Selectivity to separate CO_2 from a CO_2/CH_4 binary mixture at atmospheric pressure

For the CO_2 separation from biogas streams, selectivity factors were calculated from the multicomponent experiments carried out in the present work for a mixture of 50% CO_2-50% CH_4 at 25 ºC and 120 kPa. Selectivity factor is defined by Equation (4):

$$S_{ads} = \frac{q_1/q_2}{P_1/P_2} \quad (4)$$

where q_i is the uptake and P_i is the partial pressure of the component i [47]. The selectivity factors for the activated carbons studied in this work are shown in Table 2.

For Calgon BPL and Norit C, the CO_2/CH_4 selectivity factors calculated from the above reported breakthrough experiments were 3.20 and 3.33, respectively. For the synthesized adsorbents the CO_2/CH_4 selectivity factors under the conditions used in the present study were: 2.54 for No1KCla-600, 2.69 for No1KClb-1000 and 4.26 for No2OS-1000. Abid et al. [56] reported CO_2/CH_4 selectivity values around 3.0 and 3.5 on Zr-MOF and Zr-MOF-NH_4, respectively, at 0 ºC and 1 atm. In a recent work, Li et al. [57] designed, synthesized and tested metal-organic frameworks (MOFs) porous materials with pre-designed 'single-molecule traps' for selective adsorption of CO_2 over CH_4. In their study, the adsorption capacity of CO_2 at 23 ºC and 1 atm was found to be 4.2 mmol g^{-1}, value pointed out by the authors to be among the highest for MOFs constructed from pure carboxylate ligands.

In the present work, the CH_4 adsorption capacity of No2OS-1000 was lower than that of carbons No1KCla-600 and No1KClb-1000 (Table 2). And even though its CO_2

adsorption capacity on a mass basis was also slightly lower, the CO_2/CH_4 selectivity of the No2OS-1000 adsorbent was significantly greater. The higher the selectivity factor, the higher the purity of the product that can be expected. Therefore, the greater selectivity together with the significant CO_2 adsorption capacity on a volumetric basis of No2OS-1000 point out the enormous potential of this carbon to successfully separate CO_2 from biogas and bio-hydrogen streams. Furthermore, an additional advantage to consider is that No2OS-1000 is produced from sustainable resources, biomass wastes, and thus can be obtained at a lower cost from a renewable and relatively abundant source.

4. Conclusions

Three carbon adsorbents, No1KCla-600, No1KClb-1000 and No2OS-1000, were prepared from a phenol-formaldehyde resin, including a mixture of resin with olive stones, to be evaluated in the separation of CO_2 from bio-hydrogen and biogas streams. Breakthrough experiments consisting of six consecutive temperature swing adsorption-desorption cycles were conducted in a purpose-built lab-scale fixed-bed reactor. Two commercial activated carbons, Calgon BPL and Norit C, were also studied for comparison purposes. The phenol-formaldehyde resin-derived activated carbons showed enhanced performance compared to the reference commercial carbons, under the tested conditions: CO_2 capture capacities of up to 2.1 mmol g^{-1}, adequate CO_2/H_2 and CO_2/CH_4 selectivities and reversible adsorption. The activity of the synthesized activated carbons was maintained throughout the experiments, showing a very good cyclability and regenerability over consecutive temperature swing adsorption cycles. An increase in the CO_2 partial pressure in the CO_2/H_2 feed gas stream increased both the

CO_2 capture capacity and the breakthrough time. Eventhough, No1KCla-600 presented the greatest CO_2 uptakes, the activated carbon produced from the resin and olive stones, No2OS-1000, may be selected as the optimum for the application under study given its improved performance in terms of volumetric CO_2 uptake and CO_2/CH_4 selectivity. It holds the potential to reduce the equipment sizes in an industrial application and lower the cost of the adsorbent inventory. It can therefore be concluded that the synthesized activated carbons show promising features to be applied to the CO_2 separation from bio-hydrogen and biogas streams generated by dark fermentation.

Acknowledgements

This work was carried out with financial support from the Spanish MINECO (Project ENE2011-23467), co-financed by the European Regional Development Fund (ERDF). N.A.-G. acknowledges a FPI Predoctoral fellowship from the Spanish MINECO, co-financed by the European Social Fund.

References

[1] V. Redondas, X. Gómez, S. García, C. Pevida, F. Rubiera, A. Morán, J.J. Pis, Hydrogen production from food wastes and gas post-treatment by CO_2 adsorption, Waste Manage. 32 (2012) 60-66.
[2] M. Redwood, M. Paterson-Beedle, L. Macaskie, Integrating dark and light bio-hydrogen production strategies: towards the hydrogen economy, Rev. Environ. Sci. Biotechnol. 8 (2009) 149-185.
[3] W.-H. Chen, S.-Y. Chen, S. Kumar Khanal, S. Sung, Kinetic study of biological hydrogen production by anaerobic fermentation, Int. J. Hydrogen Energy 31 (2006) 2170-2178.
[4] X. Gómez, C. Fernández, J. Fierro, M.E. Sánchez, A. Escapa, A. Morán, Hydrogen production: Two stage processes for waste degradation, Bioresour. Technol. 102 (2011) 8621-8627.
[5] X. Gómez, A. Morán, M.J. Cuetos, M.E. Sánchez, The production of hydrogen by dark fermentation of municipal solid wastes and slaughterhouse waste: A two-phase process, J. Power Sources 157 (2006) 727-732.

[6] X. Gómez, M.J. Cuetos, J.I. Prieto, A. Morán, Bio-hydrogen production from waste fermentation: Mixing and static conditions, Renew. Energy 34 (2009) 970-975.
[7] J. Li, B. Li, G. Zhu, N. Ren, L. Bo, J. He, Hydrogen production from diluted molasses by anaerobic hydrogen producing bacteria in an anaerobic baffled reactor (ABR), Int. J. Hydrogen Energy 32 (2007) 3274-3283.
[8] M. Ferchichi, E. Crabbe, G.-H. Gil, W. Hintz, A. Almadidy, Influence of initial pH on hydrogen production from cheese whey, J. Biotechnol. 120 (2005) 402-409.
[9] Y.-W. Lee, J. Chung, Bioproduction of hydrogen from food waste by pilot-scale combined hydrogen/methane fermentation, Int. J. Hydrogen Energy 35 (2010) 11746-11755.
[10] H. Zhu, A. Stadnyk, M. Béland, P. Seto, Co-production of hydrogen and methane from potato waste using a two-stage anaerobic digestion process, Bioresour. Technol. 99 (2008) 5078-5084.
[11] X. Wang, Y.-c. Zhao, A bench scale study of fermentative hydrogen and methane production from food waste in integrated two-stage process, Int. J. Hydrogen Energy 34 (2009) 245-254.
[12] C.-F. Chu, Y.-Y. Li, K.-Q. Xu, Y. Ebie, Y. Inamori, H.-N. Kong, A pH- and temperature-phased two-stage process for hydrogen and methane production from food waste, Int. J. Hydrogen Energy 33 (2008) 4739-4746.
[13] D.-Y. Lee, Y. Ebie, K.-Q. Xu, Y.-Y. Li, Y. Inamori, Continuous H_2 and CH_4 production from high-solid food waste in the two-stage thermophilic fermentation process with the recirculation of digester sludge, Bioresour. Technol. 101 (2010) S42-S47.
[14] A. Giordano, C. Cantù, A. Spagni, Monitoring the biochemical hydrogen and methane potential of the two-stage dark-fermentative process, Bioresour. Technol. 102 (2011) 4474-4479.
[15] N. Abatzoglou, S. Boivin, A review of biogas purification processes, Biofuels Bioprod. Biorefining 3 (2009) 42-71.
[16] S.S. Kapdi, V.K. Vijay, S.K. Rajesh, R. Prasad, Biogas scrubbing, compression and storage: perspective and prospectus in Indian context, Renew. Energy 30 (2005) 1195-1202.
[17] S. Rasi, J. Läntelä, A. Veijanen, J. Rintala, Landfill gas upgrading with countercurrent water wash, Waste Manage. 28 (2008) 1528-1534.
[18] A.G. Chmielewski, A. Urbaniak, K. Wawryniuk, Membrane enrichment of biogas from two-stage pilot plant using agricultural waste as a substrate, Biomass Bioenerg. 58 (2013) 219-228.
[19] L. Deng, M.-B. Hägg, Techno-economic evaluation of biogas upgrading process using CO_2 facilitated transport membrane, Int. J. Greenh. Gas Control 4 (2010) 638-646.
[20] P. Shao, M. Dal-Cin, A. Kumar, H. Li, D.P. Singh, Design and economics of a hybrid membrane–temperature swing adsorption process for upgrading biogas, J. Membr. Sci. 413–414 (2012) 17-28.
[21] A. Alonso-Vicario, J.R. Ochoa-Gómez, S. Gil-Río, O. Gómez-Jiménez-Aberasturi, C.A. Ramírez-López, J. Torrecilla-Soria, A. Domínguez, Purification and upgrading of biogas by pressure swing adsorption on synthetic and natural zeolites, Microporous Mesoporous Mater. 134 (2010) 100-107.

[22] Y.-S. Bae, R.Q. Snurr, Development and Evaluation of Porous Materials for Carbon Dioxide Separation and Capture, Angew. Chem. Int. Ed. 50 (2011) 11586-11596.
[23] X. Wu, M. Niknam Shahrak, B. Yuan, S. Deng, Synthesis and characterization of zeolitic imidazolate framework ZIF-7 for CO_2 and CH_4 separation, Microporous Mesoporous Mater. 190 (2014) 189-196.
[24] C.A. Grande, R. Blom, A. Möller, J. Möllmer, High-pressure separation of CH_4/CO_2 using activated carbon, Chem. Eng. Sci. 89 (2013) 10-20.
[25] T. Montanari, E. Finocchio, E. Salvatore, G. Garuti, A. Giordano, C. Pistarino, G. Busca, CO_2 separation and landfill biogas upgrading: A comparison of 4A and 13X zeolite adsorbents, Energy 36 (2011) 314-319.
[26] C.A. Grande, A.E. Rodrigues, Layered Vacuum Pressure-Swing Adsorption for Biogas Upgrading, Ind. Eng. Chem. Res. 46 (2007) 7844-7848.
[27] D. Búcsú, N. Nemestóthy, Z. Pientka, L. Gubicza, K. Bélafi-Bakó, Modelling of biohydrogen production and recovery by membrane gas separation, Desalination 240 (2009) 306-310.
[28] T.-M. Liang, S.-S. Cheng, K.-L. Wu, Behavioral study on hydrogen fermentation reactor installed with silicone rubber membrane, Int. J. Hydrogen Energy 27 (2002) 1157-1165.
[29] V.V. Teplyakov, L.G. Gassanova, E.G. Sostina, E.V. Slepova, M. Modigell, A.I. Netrusov, Lab-scale bioreactor integrated with active membrane system for hydrogen production: experience and prospects, Int. J. Hydrogen Energy 27 (2002) 1149-1155.
[30] D.M. Ruthven, S. Farooq, K.S. Knaebel, Pressure swing adsorption, VCH Publishers, New York, 1994.
[31] Y. Li, H. Yi, X. Tang, F. Li, Q. Yuan, Adsorption separation of CO_2/CH_4 gas mixture on the commercial zeolites at atmospheric pressure, Chem. Eng. J. 229 (2013) 50-56.
[32] J.A.C. Silva, A.F. Cunha, K. Schumann, A.E. Rodrigues, Binary adsorption of CO_2/CH_4 in binderless beads of 13X zeolite, Microporous Mesoporous Mater. 187 (2014) 100-107.
[33] J. Yang, R. Krishna, J. Li, J. Li, Experiments and simulations on separating a CO_2/CH_4 mixture using K-KFI at low and high pressures, Microporous Mesoporous Mater. 184 (2014) 21-27.
[34] C.F. Martín, M.G. Plaza, S. García, J.J. Pis, F. Rubiera, C. Pevida, Microporous phenol–formaldehyde resin-based adsorbents for pre-combustion CO_2 capture, Fuel 90 (2011) 2064-2072.
[35] C.F. Martín, S. García, D. Beneroso, J.J. Pis, F. Rubiera, C. Pevida, Precombustion CO_2 capture by means of phenol–formaldehyde resin-derived carbons: From equilibrium to dynamic conditions, Sep. Purif. Technol. 98 (2012) 531-538.
[36] A. Knop, L.A. Pilato, Phenolic resins: chemistry, applications, and performance: future directions, Springer-Verlag, Berlin Heidelberg GmbH, 1985.
[37] A.I. Foster, H.J. Linney, S.R. Tennison, R.A. Cory, D.P. Swan, The use of carbons produced from phenolic resins for flue gas desulphurization, Fuel 72 (1993) 337-342.
[38] S.R. Tennison, Phenolic-resin-derived activated carbons, Appl. Catal. A-Gen. 173 (1998) 289-311.
[39] J. de D. López-González, F. Martínez-Vilchez, F. Rodríguez-Reinoso, Preparation and characterization of active carbons from olive stones, Carbon 18 (1980) 413-418.

[40] M.T. González, M. Molina-Sabio, F. Rodríguez-Reinoso, Steam activation of olive stone chars, development of porosity, Carbon 32 (1994) 1407-1413.
[41] M.A. Rodríguez-Valero, M. Martínez-Escandell, M. Molina-Sabio, F. Rodríguez-Reinoso, CO2 activation of olive stones carbonized under pressure, Carbon 39 (2001) 320-323.
[42] M.G. Plaza, C. Pevida, B. Arias, J. Fermoso, M.D. Casal, C.F. Martín, F. Rubiera, J.J. Pis, Development of low-cost biomass-based adsorbents for postcombustion CO_2 capture, Fuel 88 (2009) 2442-2447.
[43] M.G. Plaza, S. García, F. Rubiera, J.J. Pis, C. Pevida, Evaluation of ammonia modified and conventionally activated biomass based carbons as CO_2 adsorbents in postcombustion conditions, Sep. Purif. Technol. 80 (2011) 96-104.
[44] S. Himeno, T. Komatsu, S. Fujita, Development of a New Effective Biogas Adsorption Storage Technology, Adsorption 11 (2005) 899-904.
[45] Z. Bao, L. Yu, Q. Ren, X. Lu, S. Deng, Adsorption of CO_2 and CH_4 on a magnesium-based metal organic framework, J. Colloid Interface Sci. 353 (2011) 549-556.
[46] A. Wahby, J.M. Ramos-Fernández, M. Martínez-Escandell, A. Sepúlveda-Escribano, J. Silvestre-Albero, F. Rodríguez-Reinoso, High-Surface-Area Carbon Molecular Sieves for Selective CO2 Adsorption, ChemSusChem 3 (2010) 974-981.
[47] D.M. Ruthven, Principles of Adsorption and Adsorption Processes, Wiley, 1984.
[48] M.V. Gil, M. Martínez, S. García, F. Rubiera, J.J. Pis, C. Pevida, Response surface methodology as an efficient tool for optimizing carbon adsorbents for CO_2 capture, Fuel Process. Technol. 106 (2013) 55-61.
[49] M.M. Dubinin, Porous structure and adsorption properties of active carbons, in: P.L. Walker (Ed.), Chemistry and Physics of Carbon, Marcel Dekker Inc., New York, 1966, pp. 51-119.
[50] F. Stoeckli, L. Ballerini, Evolution of microporosity during activation of carbon, Fuel 70 (1991) 557-559.
[51] S. Brunauer, P.H. Emmett, E. Teller, Adsorption of Gases in Multimolecular Layers, J. Am. Chem. Soc. 60 (1938) 309-319.
[52] C.F. Martín, M.G. Plaza, J.J. Pis, F. Rubiera, C. Pevida, T.A. Centeno, On the limits of CO_2 capture capacity of carbons, Sep. Purif. Technol. 74 (2010) 225-229.
[53] S. García, M.V. Gil, C.F. Martín, J.J. Pis, F. Rubiera, C. Pevida, Breakthrough adsorption study of a commercial activated carbon for pre-combustion CO_2 capture, Chem. Eng. J. 171 (2011) 549-556.
[54] N. Konduru, P. Lindner, N.M. Assaf-Anid, Curbing the greenhouse effect by carbon dioxide adsorption with Zeolite 13X, AlChE J. 53 (2007) 3137-3143.
[55] C.A. Grande, R.P.P.L. Ribeiro, A.E. Rodrigues, CO_2 Capture from NGCC Power Stations using Electric Swing Adsorption (ESA), Energy Fuels 23 (2009) 2797-2803.
[56] H.R. Abid, G.H. Pham, H.-M. Ang, M.O. Tade, S. Wang, Adsorption of CH_4 and CO_2 on Zr-metal organic frameworks, J. Colloid Interface Sci. 366 (2012) 120-124.
[57] J.-R. Li, J. Yu, W. Lu, L.-B. Sun, J. Sculley, P.B. Balbuena, H.-C. Zhou, Porous materials with pre-designed single-molecule traps for CO_2 selective adsorption, Nat. Commun. 4 (2013) 1538.

Figure captions

Fig. 1. Schematic diagram of the experimental setup for the cyclic adsorption-desorption experiments.

Fig. 2. Scheme of the adsorption-desorption cycle configuration.

Fig. 3. Complete breakthrough adsorption experiments consisting of six consecutive adsorption-desorption cycles at 25 ºC and 120 kPa for 40/60 vol.% CO_2/H_2 feed gas: (a) Calgon BPL activated carbon and (b) No2OS-1000 activated carbon. (1) initial drying, (2) pre-conditioning, (3) adsorption and (4) desorption steps.

Fig. 4. Complete breakthrough adsorption experiments consisting of six consecutive adsorption-desorption cycles at 25 ºC and 120 kPa for 50/50 vol.% CO_2/CH_4 feed gas: (a) Calgon BPL activated carbon and (b) No1KClb-1000 activated carbon. (1) initial drying, (2) pre-conditioning, (3) adsorption and (4) desorption steps.

Fig. 5. CO_2 breakthrough curves of the experiments with 40/60 vol.% CO_2/H_2 (a) and 70/30 vol.% CO_2/H_2 (b) in feed gas for the activated carbons studied. (◆) cycle 1, (▲) cycle 2, (■) cycle 3, (◇) cycle 4, (△) cycle 5, (□) cycle 6.

Fig. 6. CO_2 (blue) and CH_4 (orange) breakthrough curves of the experiments with 50/50 vol.% CO_2/CH_4 in feed gas for the activated carbons: (a) Calgon BPL, (b) Norit C, (c) No1KCla-600, (d) No1KClb-1000 and (e) No2OS-1000.

Fig. 7. Breakthrough curves of the experiments with 50/50 vol.% CO_2/CH_4 in feed gas for the activated carbons studied: (a) CO_2 curves and (b) CH_4 curves.

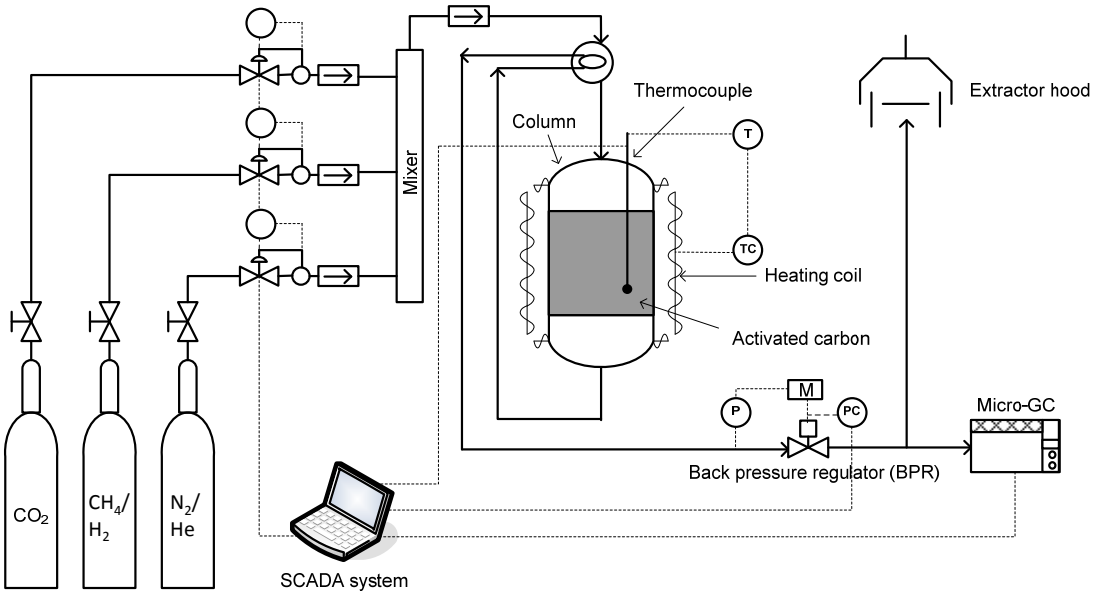
Mixer
Thermocouple
Column
T
TC
Heating coil
Activated carbon
Extractor hood
M
P
PC
Micro-GC
Back pressure regulator (BPR)
CO_2
CH_4/
H_2
N_2/
He
SCADA system

Fig. 1.

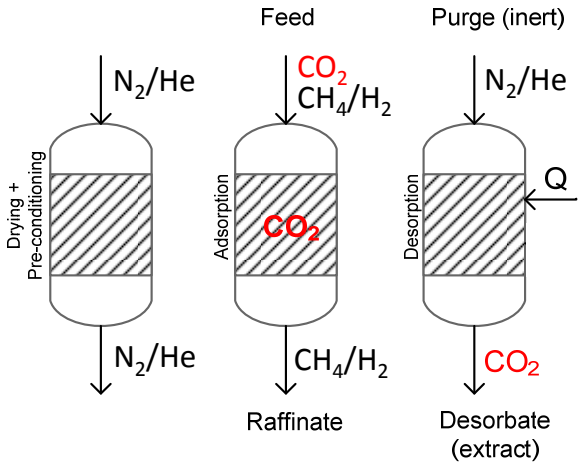
Feed
Purge (inert)
N2/He
CO2
CH4/H2
N2/He
Drying +
Pre-conditioning
Adsorption
CO2
Desorption
Q
N2/He
CH4/H2
CO2
Raffinate
Desorbate
(extract)

Fig. 2.

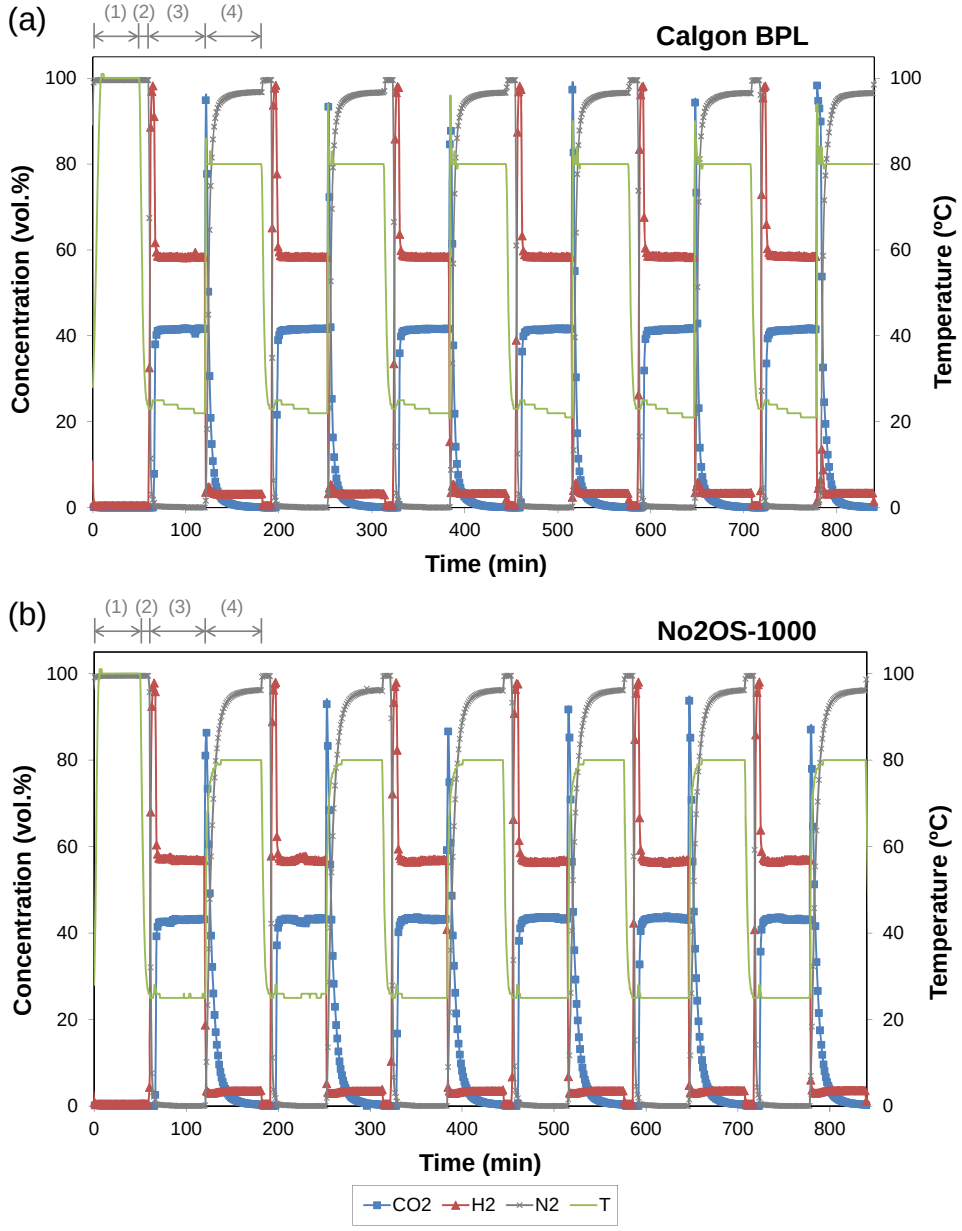
(a)
(1) (2) (3) (4)
Calgon BPL
Concentration (vol.%)
Temperature (°C)
Time (min)
(b)
(1) (2) (3) (4)
No2OS-1000
Concentration (vol.%)
Temperature (°C)
Time (min)
CO2
H2
N2
T

Fig. 3.

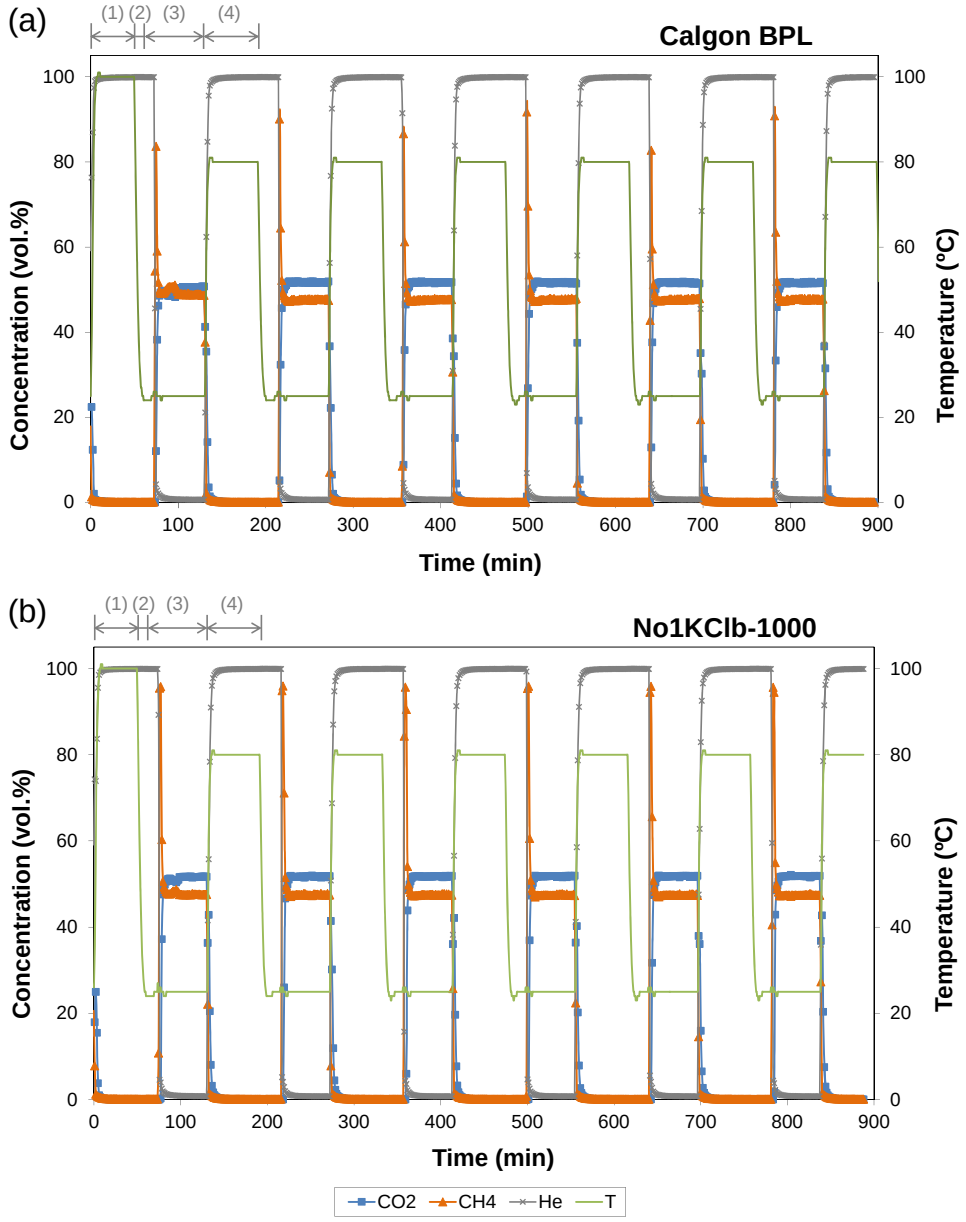
(a)
(1) (2) (3) (4)
Calgon BPL
Concentration (vol.%)
Temperature (°C)
Time (min)
(b)
(1) (2) (3) (4)
No1KClb-1000
Concentration (vol.%)
Temperature (°C)
Time (min)
CO2
CH4
He
T

Fig. 4.

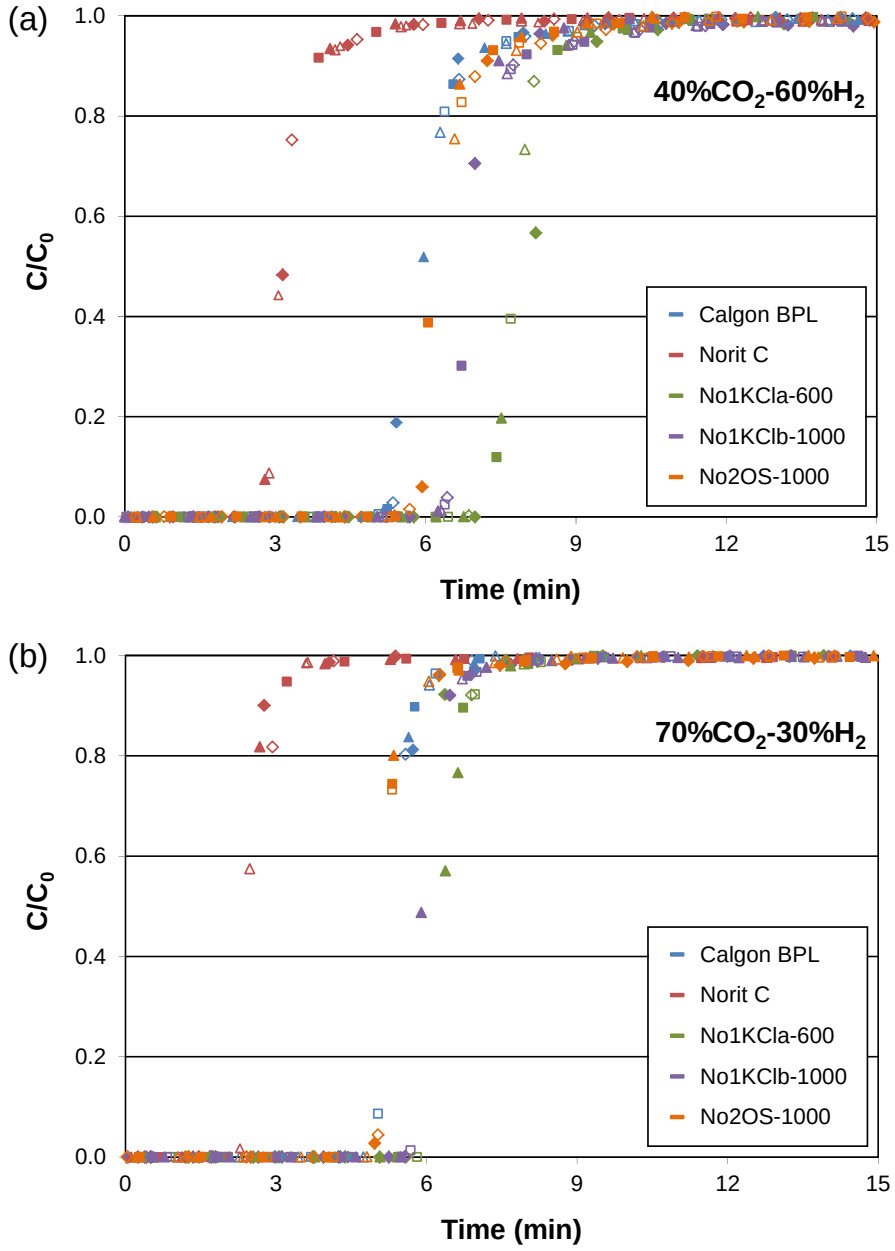
(a)
40%CO2-60%H2
C/C0
Time (min)
Calgon BPL
Norit C
No1KCla-600
No1KClb-1000
No2OS-1000
(b)
70%CO2-30%H2
C/C0
Time (min)
Calgon BPL
Norit C
No1KCla-600
No1KClb-1000
No2OS-1000

Fig. 5.

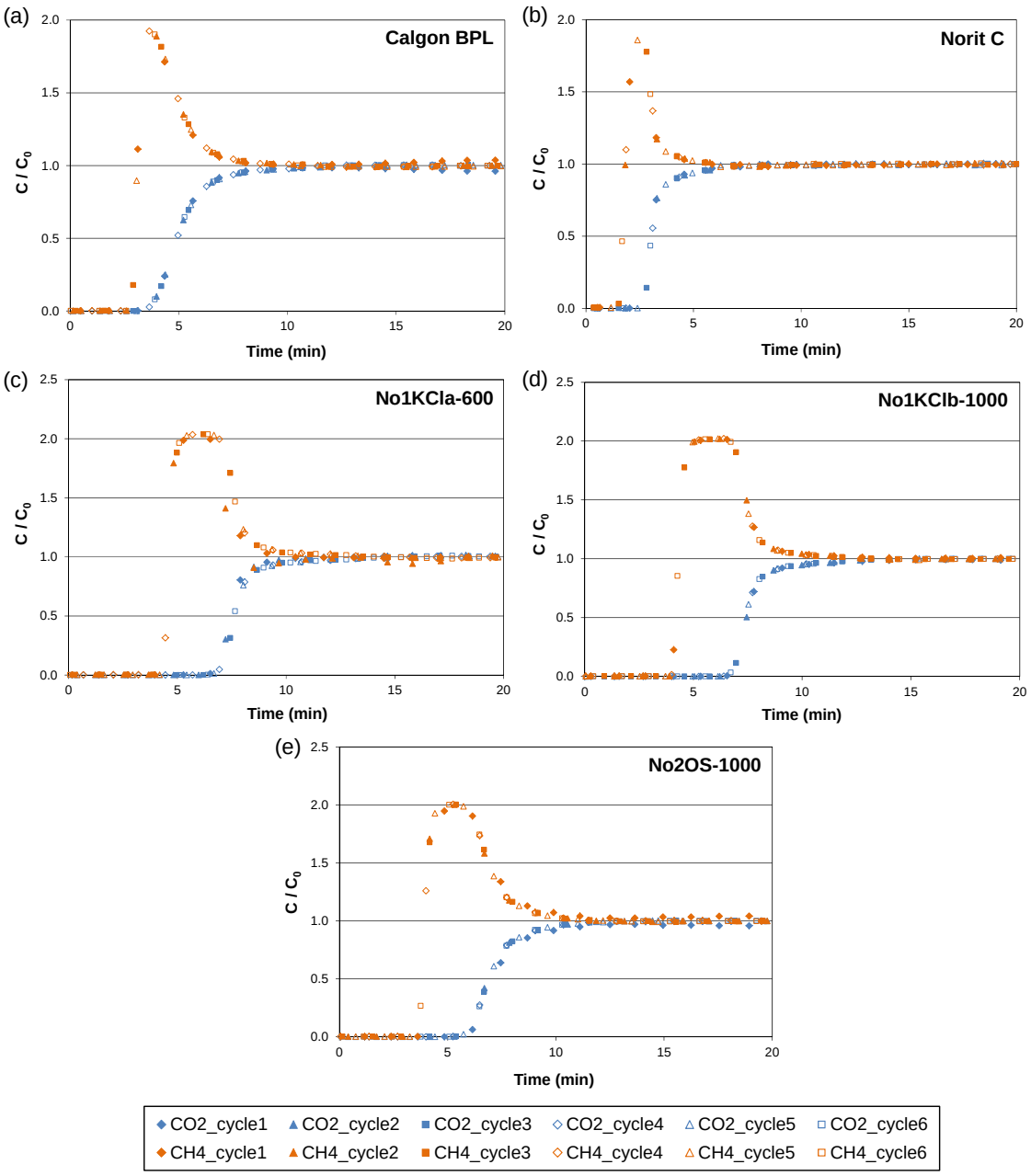
(a)
Calgon BPL
(b)
Norit C
(c)
No1KCla-600
(d)
No1KClb-1000
(e)
No2OS-1000
C / C0
Time (min)
CO2_cycle1
CO2_cycle2
CO2_cycle3
CO2_cycle4
CO2_cycle5
CO2_cycle6
CH4_cycle1
CH4_cycle2
CH4_cycle3
CH4_cycle4
CH4_cycle5
CH4_cycle6

Fig. 6.

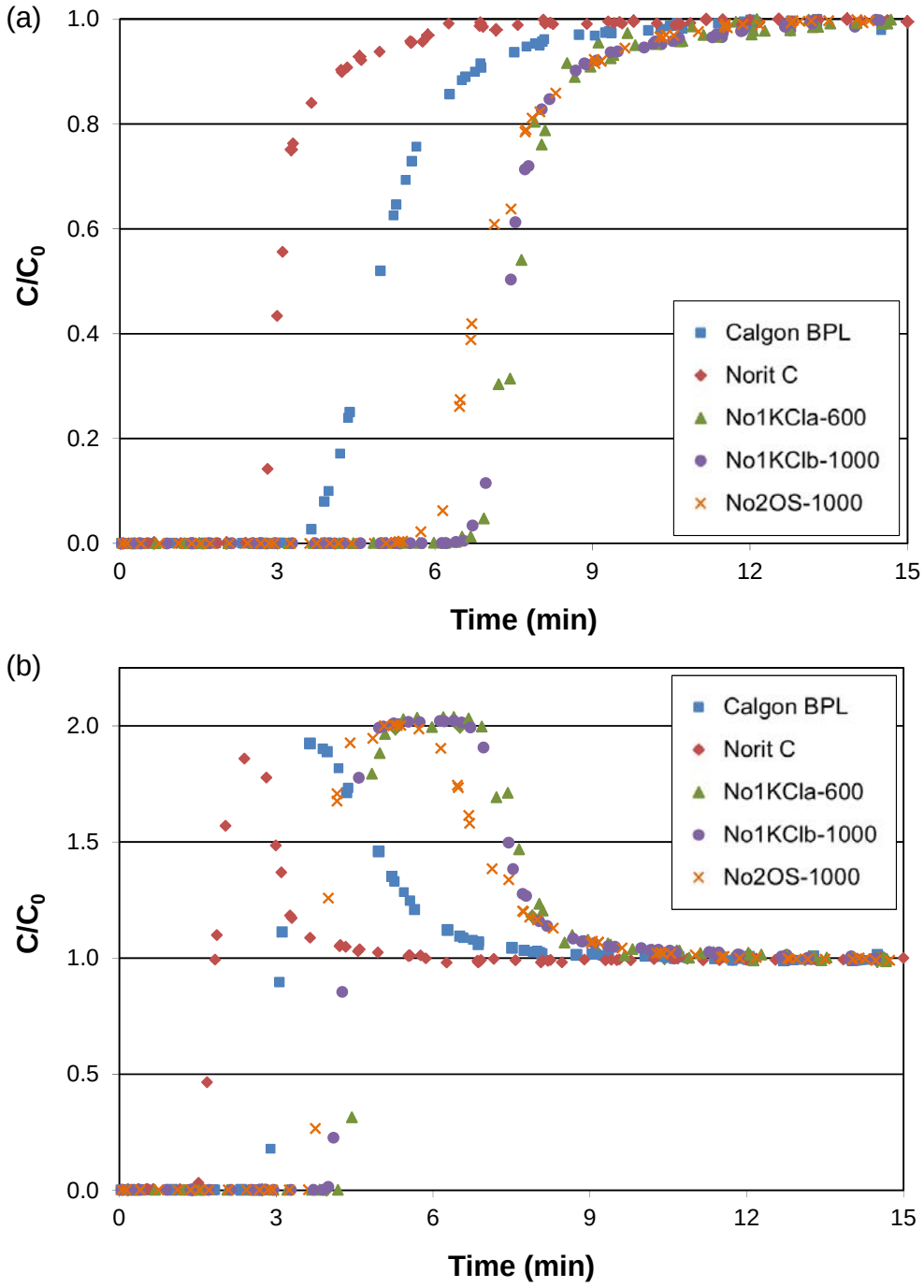
(a)
1.0
0.8
0.6
0.4
0.2
0.0
C/C0
0
3
6
9
12
15
Time (min)
Calgon BPL
Norit C
No1KCla-600
No1KClb-1000
No2OS-1000
(b)
2.0
1.5
1.0
0.5
0.0
C/C0
0
3
6
9
12
15
Time (min)
Calgon BPL
Norit C
No1KCla-600
No1KClb-1000
No2OS-1000

Fig. 7.

Table 1. Physical properties of the activated carbons and bed characteristics.

	Activated carbon				
	Calgon BPL	Norit C	No1KCla-600	No1KClb-1000	No2OS-1000
N_2 adsorption at -196 ºC					
BET surface area ($m^2 g^{-1}$)	1129	1361	1091	804	1233
Total pore volume ($cm^3 g^{-1}$)	0.50	0.97	0.42	0.32	0.53
Micropore volume ($cm^3 g^{-1}$)[a]	0.46	0.51	0.40	0.32	0.50
Average micropore width (nm)[b]	1.4	2.9	1.0	1.2	0.8
CO_2 adsorption at 0 ºC					
Narrow micropore volume ($cm^3 g^{-1}$)[a]	0.22	0.22	0.35	0.29	0.33
Average narrow micropore width (nm)[b]	0.70	0.74	0.7	0.6	0.7
Mass of adsorbent (g)	2.68	1.53	2.59	2.54	2.84
Particle size (mm)	2-4.75	0.85-1.7	1-3	1-3	1-3
Total porosity, ε_T	0.79	0.85	0.84	0.85	0.79
Helium density ($g\ cm^{-3}$)[b]	2.10	1.51	1.89	1.90	2.02
Apparent density ($g\ cm^{-3}$)[c]	0.83	0.40	1.13	1.11	0.75
Bed diameter (cm)	0.9	0.9	0.9	0.9	0.9
Bed height (cm)	9.7	10.7	13.3	13.8	10.7
Bed density ($g\ cm^{-3}$)	0.432	0.225	0.307	0.289	0.419

[a] Evaluated with the Dubinin-Radushkevich equation.
[b] Determined with the Stoeckli-Ballerini relation.
[b] Determined by He picnometry.
[c] Determined by Hg porosimetry.

Table 2. CO_2 and CH_4 adsorption capacities from the breakthrough experiments at 25 ºC and 120 kPa.

Feed composition	CO_2 adsorption capacity					CH_4 adsorption capacity				Selectivity CO_2/CH_4
	(mol/kg adsorbent)	(wt.%)	(kg/m^3)	t_b (min)	% unused bed	(mol/kg adsorbent)	(wt.%)	(kg/m^3)	t_b (min)	
40%CO_2/60%H_2										
Calgon BPL	1.07	4.72	20.39	5.18	17.39					
Norit C	0.97	4.27	9.61	2.31	33.38					
No1KCla-600	1.57	6.92	21.24	6.73	13.76					
No1KClb-1000	1.49	6.56	18.95	6.24	14.07					
No2OS-1000	1.17	5.15	21.61	5.40	15.21					
70%CO_2/30%H_2										
Calgon BPL	1.49	6.55	28.33	4.44	20.14					
Norit C	1.02	4.49	10.09	1.64	29.20					
No1KCla-600	2.11	9.26	28.43	5.55	12.32					
No1KClb-1000	2.04	8.99	25.95	5.42	12.43					
No2OS-1000	1.74	7.64	32.03	4.54	19.49					
50%CO_2/50%CH_4										
Calgon BPL	1.47	6.45	27.89	3.40	-	0.46	2.01	8.68	2.20	3.20
Norit C	1.50	6.60	14.84	2.09	-	0.45	1.96	4.41	0.98	3.33
No1KCla-600	2.03	8.92	27.36	6.65	-	0.80	3.52	10.79	3.85	2.54
No1KClb-1000	1.91	8.39	24.22	6.42	-	0.71	3.11	8.98	3.61	2.69
No2OS-1000	1.83	8.06	33.81	5.52	-	0.43	1.90	7.96	2.91	4.26

t_b: breakthrough time.